Elastic neutron scattering of the "phase ordering" phase transition in $Hg_{3-\delta}AsF_6$

J. P. Pouget,* G. Shirane, and J. M. Hastings
Brookhaven National Laboratory, Upton, New York 11973

A. J. Heeger,† N. D. Miro,‡ and A. G. MacDiarmid‡
Laboratory for Research on the Structure of Matter, University of Pennsylvania, Philadelphia, Pennsylvania 19104
(Received 16 May 1978)

Elastic-neutron-scattering experiments performed on the linear-chain mercury compound $Hg_{3-\delta}AsF_6$ are presented. On cooling, a progressive phase ordering between the Hg chains, randomly phased at room temperature, has been found and characterized. Short-range order gradually builds up, with transverse coherence lengths of a few lattice constants, as a result of parallel chain-chain interactions. At 120 K, the competing orthogonal chain-chain interaction leads to three-dimensional order and a phase-ordering phase transition. The three-dimensional low-temperature phase is accompanied by an incommensurate modulation of the Hg chains indicating an interaction with the host lattice.

I. INTRODUCTION

The discovery of the remarkable electronic and structural properties[1] exhibited by the growing class of anisotropic, quasi-one-dimensional conductors has generated considerable interest in the study of these compounds and in the general area of research on anisotropic metals with chainlike structures. Recently, a new group of anisotropic metals containing infinite chains of mercury ions has been reported.[2-4] The polymercury cation compounds $Hg_{2.86}AsF_6$ (hereafter $Hg_{3-\delta}AsF_6$) and $Hg_{2.91}SbF_6$ have anisotropic electrical conductivities[5,6] and anisotropic optical properties[7,8] consistent with relatively weak interchain electronic coupling. The $Hg_{3-\delta}AsF_6$ compound remains metallic to low temperatures[5,6,9] with no indication of residual resistance,[6] and has a linear term in the specific heat[10] which is unusually large compared to that expected from the electronic density of states.[9] Below 4.1 K, $Hg_{3-\delta}AsF_6$ becomes an anisotropic superconductor[6] in low magnetic fields and exhibits an anisotropic Meissner effect.[11]

The crystallographic structure of the $Hg_{3-\delta}AsF_6$ compound has been determined at room temperature by Brown *et al.*[3] and confirmed by Schultz *et al.*[12] using neutron diffraction. This compound has a body-centered tetragonal space group $I4_1/amd$ (D_{4h}^{19}) with four formula weights of $Hg_{3-\delta}AsF_6$ per unit cell. For a better understanding of this structure it is convenient to separate the lattice in two parts: the host lattice (AsF_6 lattice) and the mercury chains. The host lattice is made up of a body-centered tetragonal array of well separated AsF_6 octahedra. Figure 1 presents a drawing of this lattice of octahedra as generated by computer program[13] using the crystallographic refinement of Brown *et al.*[3] The parallel projection along the [100] direction has been done without perspective to give a clearer view of the size (≃ 5Å in diameter) and of the array of channels running along this direction. The noninteracting channels in the [100] and [010] directions, equivalent by tetragonal symmetry, are indicated by the full lines. Figure 2 presents, in a more schematic manner, the position of these channels in the AsF_6 unit cell. This cell is crossed by two channels running in the [100] direction with coordinates, based on the host lattice, of (0, 0) and (0.5, 0.5) in the (100) plane and two channels running along the [010] direction with coordinates

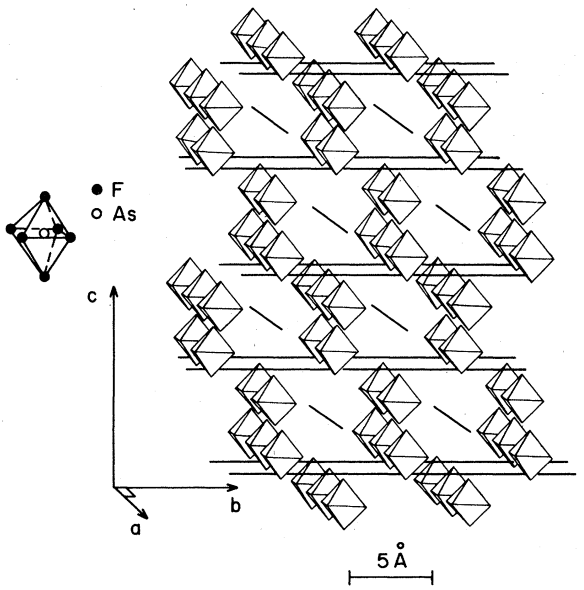

FIG. 1. Schematic drawing of the $Hg_{3-\delta}AsF_6$ structure. The tetragonal axis system is indicated in the lower left corner. The Hg chains are shown as solid lines.

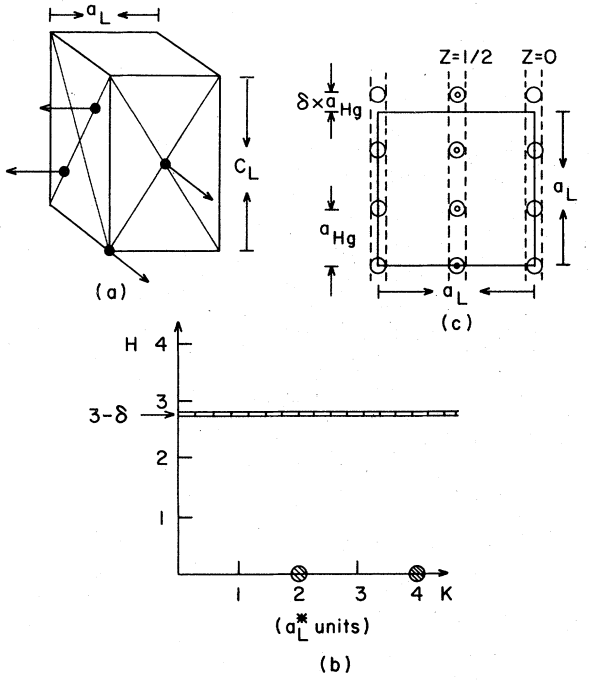

FIG. 2. (a) Unit cell of $Hg_{3-\delta}AsF_6$ indicating positions of the mercury chains. (b) *(h0l)* plane in reciprocal space. The shaded line at $H = 3 - \delta$ is the intersection of this plane with the diffuse scattering sheet associated with the set of parallel Hg chains represented in (c). The spots along the K axis are Bragg reflections to which both the AsF_6 and Hg sublattices contribute. (c) Basal plane projection of Hg chains parallel to the [100] direction. The dotted lines along the chains mean that there is no phase order between chains.

(0.25, 0.25) and (0.75, 0.75) in the (010) plane. Infinite chains of mercury atoms lie within these channels. There are no mercury chains along the c axis.

The surprise of the x-ray investigation of Brown *et al.*[3] was the discovery that in addition to the Bragg reflections in reciprocal space there are two sets of equidistant sheets of very strong diffuse intensity. This is clearly shown by the x-ray diffuse scattering pattern presented in Fig. 3(a)[14]; the two sets of intense diffusion lines come from the intersection of the Ewald sphere with the two orthogonal sets of diffuse sheets. Brown *et al.*[3] associated each direction of diffuse sheet with the corresponding direction of the linear channel in real space. The diffuse intensity arises from the mercury atoms, and its distribution in a sheet is explained if there is no phase coherence between the neighboring chains. These diffuse sheets are therefore viewed as Bragg reflections from a one-dimensional (1D) lattice.

Figure 2(c) summarizes the above results, presenting for clarity only one direction of chains:

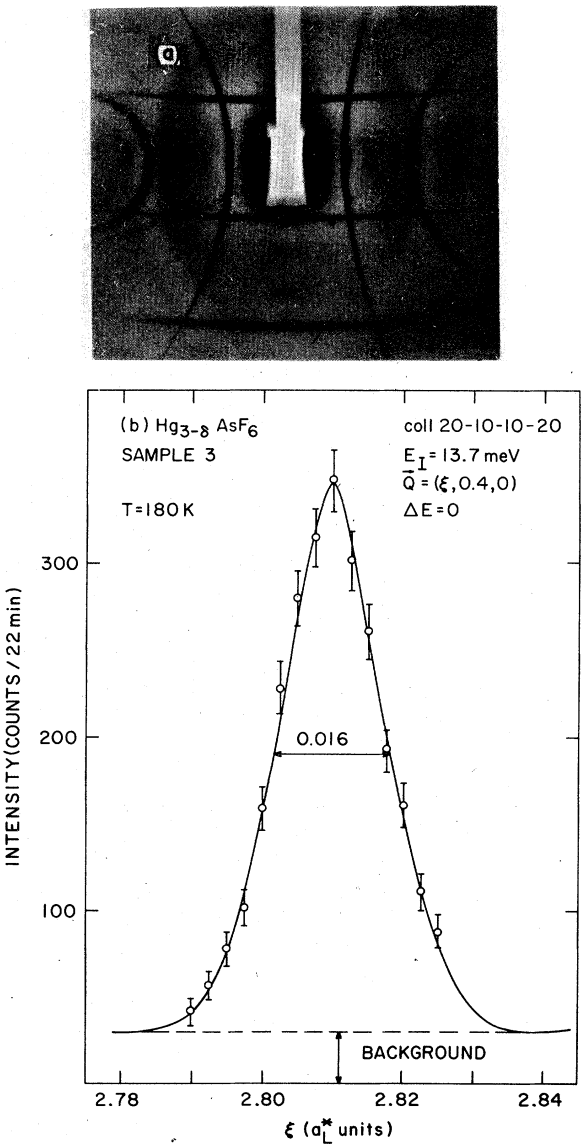

FIG. 3. (a) Diffuse x-ray pattern of $Hg_{3-\delta}AsF_6$ at room temperature. The incident beam is along the c_L^* direction (the subscript L refers to the host lattice). The curvature of the lines is the result of the flat plate geometry of the film (from Ref. 14). (b) (ξ, 0.4, 0) elastic neutron scan through the first diffuse sheet at 180 K. The width is resolution limited indicating an intrachain coherence length greater than 400 Å.

(i) the Hg atoms are well ordered along the chain direction. (ii) The intrachain mercury distance a_{Hg} is incommensurate with the host lattice parameter a_L along the chain direction. (iii) There is no phase order among neighboring chains. (iv) There is periodicity in position of the Hg chains, imposed by the regular network of open channels of

the host AsF_6 sublattice.

The commensurate relation between the positions of the Hg chains and the host lattice, as expressed by this last point, explains why no diffuse sheet passing through the origin of reciprocal space is observed [see Fig. 3(a)]. This intensity can be viewed as coalesced into Bragg spots in the $(0kl)$ plane, for the mercury chain parallel to the [100] direction. Generally there will be contributions from both Hg and AsF_6 sublattices to these Bragg spots. The same is true in the $(h0l)$ plane for the mercury chains parallel to the [010] direction. From the position of the atoms in the unit cell,[2] it is easy to see that the Hg atoms contribute to the Bragg reflection with $k+l=2n$ and the AsF_6 octahedra to the Bragg reflection with $2k+l=2n+1$ or $4n$ in the $(0kl)$ plane (n is an integer). Some of these reflections along the [010] direction, with contribution from both sublattices are also shown in Fig. 2(b). We note, however, that there are Bragg reflections like (022), (042), (062) where only the Hg chains contribute.

A crystallographic structure composed of two incommensurate sublattices has been observed in some tetrathiafulvalene (TTF) salts like $(TTF)Br_x$,[15] and $(TTF)I_x$.[16] However, the polymercury cation compounds are unique in the sense that only the anionic sublattice forms a three-dimensional (3D) lattice; the mercury chains forming a set of 1D lattices without any phase relation between them. This unique structural feature requires a more extensive study of the behavior of the mercury chains, particularly when the temperature is lowered.[17]

Analysis of the crystal growth[18] leads to the conclusion that mass transport of the mercury atoms occurs along the chain channels at room temperature. Thus the atoms are mobile, and the presence of interchain interactions can be expected to lead to phase ordering of the mercury chains. Denoting U_i ($=U_\parallel$ or $U_\perp$) as the interaction between chains (parallel or perpendicular), we expect interchain order at temperatures when $U_i \xi / a_{Hg} \simeq kT$ where ξ is the correlation length along the chain. The detailed nature of the low-temperature ordered state will depend on the relative strengths of the parallel chain and perpendicular chain interactions. In general, the two kinds of interactions will lead to different order, and thus compete in the region above the phase transition. Experimentally the perpendicular chain coupling is found to dominate at low temperatures with parallel chain short-range order playing an important role at intermediate temperatures.

A brief report of the observations in $Hg_{3-\delta}AsF_6$ by neutron scattering of the "phase ordering" phase transition, the precursor short-range order at higher temperatures, and the 1D phonon spectrum at room temperature has been published.[17] Since much more detailed data are now available, we give in this paper an extended study of $Hg_{3-\delta}AsF_6$ by elastic neutron scattering. The experimental conditions are given in Sec. II. The temperature dependence of the crystallographic structure is described in Sec. III, with emphasis on the particular features of importance at lower temperatures where phase correlations begin to develop between mercury chains. A general survey of these low-temperature results and their temperature dependence is included in Sec. III. A more precise description of the phase coupling between the mercury chains is presented in Sec. IV. Finally, the important results of this study are summarized in Sec. V.

II. EXPERIMENTAL

A. Experimental procedure

The elastic-neutron-scattering measurements were performed on a triple-axis spectrometer at the Brookhaven high-flux beam reactor. To remove the inelastic background and to improve the resolution in $\vec{Q}$ space we have used the spectrometer in the $E=0$ analyzing mode. Two different ranges of energy for the incident neutron beam were used. The first was at an incident energy (E_i) of 13.7 or 14.8 meV with pyrolytic graphite as monochromator, filter, and analyzer. Most of the experiments were done with these energies. The second was an E_i of 47.3 meV with beryllium crystals as monochromator and analyzer. This energy was chosen for a larger survey of the reciprocal space with a reduced absorption of the Hg nucleus.

B. Samples

The three single-crystal samples used during this study were grown at the University of Pennsylvania by the method described in Ref. 18. They were beautifully well faceted and silvery golden in appearance with dimensions $32\times32\times2$ mm^3 (sample 3). The lattice constants of these three samples, at room temperature, are $a=7.534(7)$ Å and $c=12.395(8)$ Å which are in good agreement with previous results.[3,12] They appear well ordered, with the mosaic spread of the main Bragg peaks being less than the resolution of the spectrometer (0.2° FWHM). Sample 1 was oriented with $(h0l)$ as scattering plane and samples 2 and 3 with $(hk0)$ as scattering plane. As $Hg_{3-\delta}AsF_6$ reacts with air, the samples were mounted under high quality He in a controlled atmosphere dry

box. After several cycles in temperature, samples 1 and 3 were broken. Sometimes we have observed, around 220 K, a splitting of the (200) Bragg reflection which often recovered when going outside this temperature range. This effect, which does not affect the temperature behavior of the mercury diffuse sheets, has not been studied in detail, but it is worth noting that the electrical conductivity seems to exhibit a small anomaly[5,6] in this temperature region. The greatest part of our results, concerning the Hg chains, have been obtained below 180 K.

III. TEMPERATURE DEPENDENCE OF THE ELASTIC DIFFUSE SCATTERING

Having described the structure of the compound at room temperature, we present here the behavior of the diffuse sheets on cooling down. Since in the tetragonal structure the two directions of chains are equivalent by symmetry, we report only the behavior of one set of diffuse sheets and more particularly the $(3-\delta, k, 0)$ diffuse line discussed above and shown in Fig. 2(b). We shall consider its width, its position, and the distribution of the intensity along k both at room temperature and when the temperature is decreased.

Important information, concerning the spread of the order of the Hg atoms within individual chains, can be obtained by measuring the width of the sheet. Scanning along the [100] direction, for different temperatures ranging from room temperature to 30 K, we have always found a resolution limited width for the first sheet. With the incident energy $E_i = 13.8$ meV and the tightest collimation possible, at 180 K, we obtain a resolution limited width, $\Delta_{FWHM} = 0.016\, a_L^*$, as shown in Fig. 3(b). Taking this value as a lower bound for the 1D order along the chain direction, we get a length $(\xi_{\parallel} = 2\pi/\Delta_{FWHM})$ in excess of 400 Å or 150 Hg-Hg spacings. At the scale of our resolution, there is long-range order of the mercury atoms in the chain direction at all temperatures.

Since the diffuse sheets can be viewed as Bragg reflections from a 1D lattice, one can obtain the intrachain repeat Hg-Hg distance a_{Hg} from the distance between sheets. The relation between a_{Hg}, the host lattice tetragonal parameter a_L, and the stoichiometry quantity δ, is given by

$$a_{Hg} = a_L/3-\delta\,. \qquad (1)$$

At room temperature, we have observed (in the units of the reciprocal space of the host lattice) the first and second sheets on three separate crystals at the respective positions $H = 2.822 \pm 0.005$ and $H = 5.690 \pm 0.007$, which results in an intrachain Hg-Hg distance a_{Hg} of 2.670 ± 0.005 Å. This distance is slightly larger than the 2.64 ± 0.02 Å determined previously by x-ray[3] and neutron diffraction[7] using a similar method. The important point is that the a_{Hg} distance is not commensurate with the host lattice parameter a_L. Per channel and unit cell, there is a mean occupation of $3-\delta$ mercury atoms, giving the empirical $Hg_{3-\delta}AsF_6$ quoted since the beginning of this article; at room temperature $\delta = 0.18$. However, the resulting formula, $Hg_{2.82}AsF_6$, deduced from these structural measurements is not in good agreement with that obtained from an elemental analysis[18] where the results indicate stoichiometric composition Hg_3AsF_6.

The resolution of the apparent conflict in the structural and analytical results appears to be in the existence of a defect structure with approximately one AsF_6 in twenty missing from the structure.[12] The resulting chemical formula expressed per average unit cell would be $Hg_{2.82}(AsF_6)_{0.94}$. Precision density measurements[18] have confirmed this picture. The measured density is found to be $\rho_{meas} = 7.05 \pm 0.01$ g/cm^3, in close agreement with the calculated value $\rho_{calc} = 7.04$ g/cm^3 based on the known structure and the above formula. An alternative suggestion of 6% excess Hg disordered in the lattice would lead to a density of 7.49 g/cm^3. Thus, the mercury chain salt is apparently a stoichiometric compound in an incommensurate structure.

The temperature dependence of the host lattice constant a_L and the position of the first diffuse sheet with respect to the host reciprocal lattice constant, $3-\delta$, are given in Fig. 4. The parameter a_L shows a relatively large contraction of 1% between room temperature and 10 K. A similar contraction of the c_L lattice parameter is observed; c_L decreases from 12.395 Å at room temperature to 12.248 Å at 10 K.

The temperature dependence of the Hg stoichiometry, $3-\delta$ entering in the empirical formula $Hg_{3-\delta}AsF_6$ is deduced from the scattering measurements. The observed variation in fact reflects completely that of the host lattice parameters a_L. The position of the diffuse sheets are (within experimental error) constant in reciprocal space at all temperatures giving a temperature-independent Hg-Hg repeat distance: $a_{Hg} = 2.670(5)$ Å. This change in $3-\delta$, reversible in temperature and reproducible over several cycles, poses an interesting question concerning the behavior of the Hg atoms in the chains on cooling down. Several possibilities must be considered: 1% of the Hg atoms flow out of the channels onto the surface of the sample; 1% of the Hg atoms go into interstitial positions or into the AsF_6 vacancy sites des-

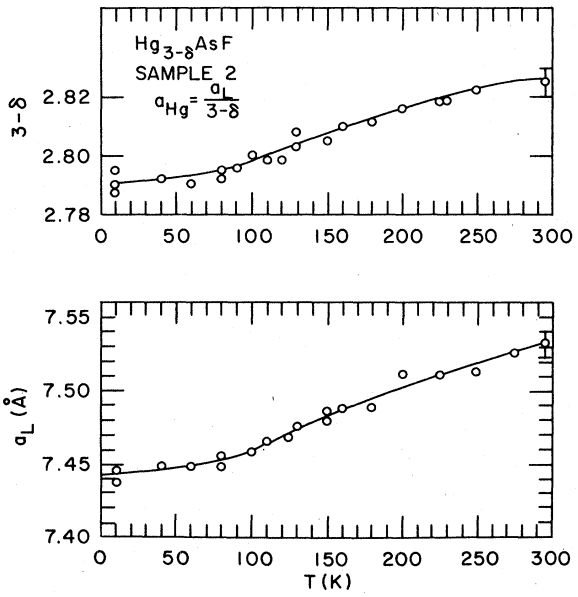

FIG. 4. Temperature dependence of the position $3-\delta$, of the first sheet and of the lattice parameter a_L for sample 2.

cribed above.

Direct visual observation of single crystals cooled to 77 K in a glass bulb showed a few tiny mercury droplets appearing on the surface. However, quantitative measurements[18] with a calibrated microscope indicated that no more than about 10^{-4} volume fraction of Hg was coming out. A probable explanation for this excess is the partial occupation of anion vacancy sites.

Extensive measurements were made to characterize the temperature dependence of the Hg chain-chain correlations. The distribution of intensity in the $(hk0)$ zone has been measured at a variety of temperatures. Figure 5 presents elastic scans along the diffuse line $(3-\delta, \eta, 0)$. The room-temperature scan shows that within experimental errors the distribution of the intensity proves directly that there is no phase relation between the mercury positions among neighboring chains. As the temperature is lowered the effect of the chain-chain interactions leads to a modulation of the uniform intensity. Slowly at the beginning, and more rapidly below 180 K, large peaks centered around $\eta \simeq 0.4$, grow in intensity; while at the same time a decrease of the scattered intensity around $\eta \sim \pm 1$ is observed. A brief survey along the diffuse line $(3-\delta, \eta, 1)$ shows that the intensity builds up around $\eta \simeq \pm 0.6$. This can be reconciled with $\eta \simeq \pm 0.4$ for $l = 0$ by indexing these peaks as $[h(3-\delta), k \pm 0.6, l]$ with $h+k+l = 2n$. Thus, the peaks observed on the line $(3-\delta, \eta, 0)$ should properly be indexed as $(3-\delta, 1 \pm 0.6, 0)$.

The intensity of the maximum of the $(3-\delta, 0.4, 0)$ peaks are replotted with more experimental points in Fig. 6. It increases until 125 K, then drops abruptly by a factor of 2 in the five following degrees. Below 120 K, the decrease continues, but somewhat more slowly. At 10 K, the peak is still barely visible, but away from ± 0.4, the data in Fig. 5 show that the diffuse sheet has nearly reached the background level. The sharper peaks at the $\eta = 1 \pm \delta$ and $\eta = -1 \pm \delta$ positions begin to appear at 150 K (see Fig. 5) and increase strongly in intensity on cooling. The temperature

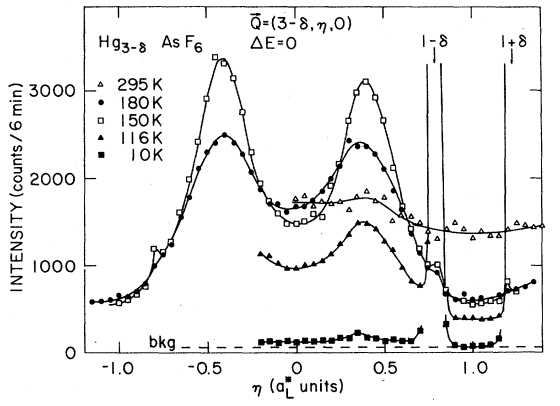

FIG. 5. Elastic scans along the diffuse line $(3-\delta, \eta, 0)$ shown in Fig. 2(b) for different temperatures. The coherent peaks at $1 \pm \delta$ are off scale in this figure.

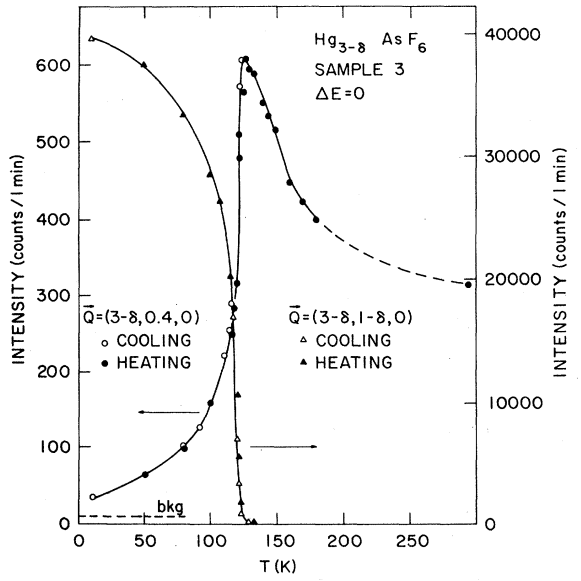

FIG. 6. Temperature dependence of the $(3-\delta, 0.4, 0)$ and $(3-\delta, 1-\delta, 0)$ peak intensity on heating (solid points) and cooling (open points).

dependence of the intensity of the $(3-\delta, 1-\delta, 0)$ peak is also presented in Fig. 6. A dramatic increase of the intensity of this peak occurs near 120 K, indicative of a true phase transition. The intensities at $(3-\delta, 0.4, 0)$ and $(3-\delta, 1-\delta, 0)$ have been plotted in Fig. 6, for comparison, to show the correlation in temperature between the drop in intensity of the first peak and the increase of the intensity of the second one. There is a transformation from one type of order to another which will be discussed in more detail later.

The scans presented in Fig. 5 show that the $(3-\delta, \pm 0.4, 0)$ peaks remain broad at all temperatures with width varying from $0.5\, a_L^*(T=180$ K) to $0.3\, a_L^*(T=120$ K). In contrast, the $(3-\delta, 1\pm\delta, 0)$ peaks are always narrow. Although it is difficult to determine precisely the width of these peaks which first appear around 150 K, they are resolution limited in width at all temperatures below 130 K.

This phase transformation is shown in greater detail in Fig. 7 where the temperature dependence of the intensity of the $(3-\delta, 1-\delta, 0)$ peak is plotted on cooling and heating. The transition is continuous in temperature, but extremely sluggish: after a temperature change of 0.25 K in this region, about 45 min are needed to reach equilibrium. It is important to note that the degree of transformation between the two types of order is extremely sensitive to the speed with which one passes through this temperature region. Cooling more rapidly "freezes" in the short-range order; the $(3-\delta, 0.4, 0)$ reflectance remains strong even at 10 K. Because of the long intrachain coherence length, interchain phase shifts require motion of entire Hg chains with respect to one another. Thus, it is qualitatively understandable that the phase ordering transition at this relatively low temperature (for ionic motion) of 120 K should be sluggish. Moreover, since the two types of order, i.e., $(3-\delta, 0.4, 0)$ and $(3-\delta, 1\pm\delta, 0)$, are physically quite different (see Sec. IV), rapid cooling will cause the high-temperature short-range order to be frozen in. The tail shown in Fig. 7 above 125 K, is probably, in part, the result of sample inhomogeneities rather than critical scattering associated with the transition. Evidently the local phase ordering is very sensitive to the local invironment with impurities, vacancies, and defects resulting in a distribution of interchain coupling and a corresponding spread of the transition.

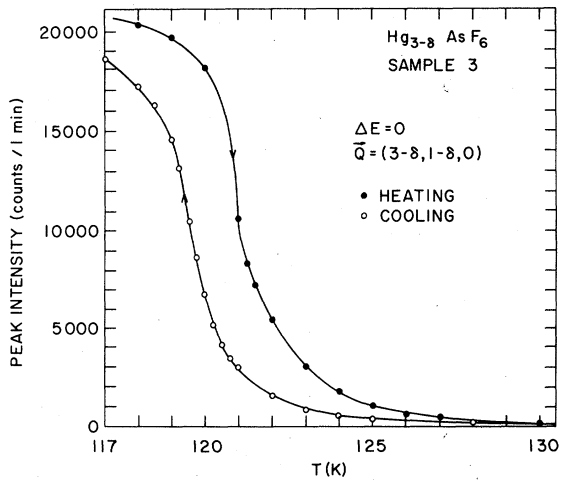

FIG. 7. Temperature dependence arount 120 K of the peak intensity of the $(3-\delta, 1-\delta, 0)$ Bragg reflection. Note the hysteresis of about 1.5 K between the cooling (open points) and heating (closed points) curves.

The data on Fig. 6 suggest that the transformation between the two types of order is quasireversible in temperature. In fact, with an expanded temperature scale, Fig. 7 shows clearly an hysteresis of about 1.5 K. By cycling the temperature in this region, it is also possible to draw hysteresis loops. The different paths followed by the cooling and heating curves suggest that the interchain phase has relative minima associated with each of the two types of order, and that the transformation between them is nearly first order.

IV. TYPES OF PHASE ORDER BETWEEN THE MERCURY CHAINS

In this section, we propose possible models to explain the observed diffraction effects in both the short-range and long-range-order regimes. At room temperature, the individual mercury chains may be considered as one-dimensional liquids, i.e., there is a fixed Hg-Hg separation but the position of the mercury ions along any chain is random relative to the host lattice. On cooling, the relative positions of the mercury ions in neighboring chains start to show a correlation leading eventually to long-range order.

A. Short-range order

There are two basic features in the scattering arising from the short-range order which develops below room temperature. The first, illustrated in Fig. 5, is the appearance of broad peaks at $\eta=\pm 0.4$ in a scan along $(3-\delta, \eta, 0)$ in the first sheet. The other feature is that a similar scan along $(6-2\delta, \eta, 0)$ in the second sheet shows no peaks even at 130 K where the first sheet is most strongly peaked.

The development of the broad peaks at $\eta=\pm 0.4$ is caused by the parallel chain-chain interaction

which leads to a correlation of the relative positions or phases of the mercury ions in neighboring chains. The form of the correlation is illustrated in Fig. 8. The upper section of the figure shows a basal plane projection of the mercury chains parallel to the [100] direction which would produce a peak at $\eta = +0.4$. The structure shows a phase shift of 0.6 a_{Hg} between chains at the $z = 0$ level while the phase shift between chains at the $z = \frac{1}{2}$ level is such that the monoclinic unit cell, outlined by the dashed lines, is body centered. The reciprocal-space diagram corresponding to this structure is illustrated in the lower half of Fig. 8. Thus, for the first sheet ($h = 1$) we can account for the $(3 - \delta, 0.4, 0)$ peak of Fig. 5. A phase shift, in a different region or domain of the crystal, of $-0.6\ a_{Hg}$ will lead to a peak at $(3 - \delta, -0.4, 0)$.

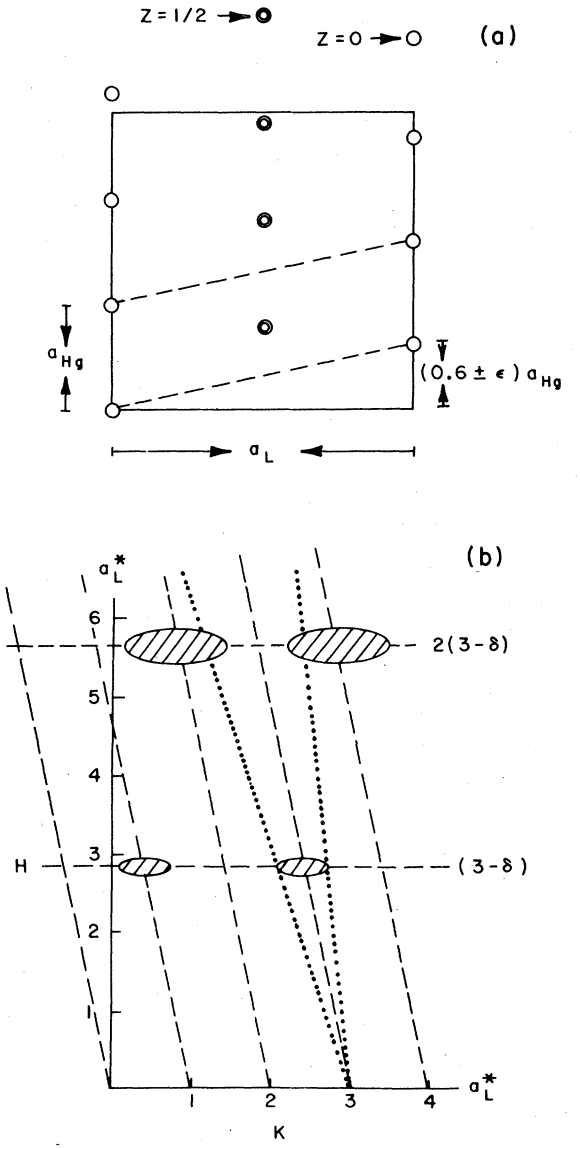

FIG. 8. (a) Basal plane projection of Hg chains parallel to the [100] direction showing the correlation of position or phase between chains in the short-range-order regime. (b) Reciprocal-space diagram corresponding to (a). The dotted lines indicate the Q-dependent broadening produced by superimposing positional disorder on the phase shift.

The observed width of these broad peaks decreases only slightly with decreasing temperature over the whole short-range-order regime as can be seen from Fig. 5. The intensity, on the other hand, shows a large increase over the same temperature interval and, as the data in Fig. 6 indicate, would appear to be diverging with a "virtual" critical temperature somewhat below 120 K. The persistent broadness of the peaks indicates that the size of the phase-correlated regions increases only slightly with decreasing temperature. This, in turn, implies that the structure of the short-range order is somehow incompatible with the development of long-range order. The increase of intensity probably comes about from an increase in the number of these correlated regions.

The other feature of the short-range-order scattering referred to above is the absence of any structure in the second sheet, $h = 2(3 - \delta)$. The model considered so far leads to a uniform broadening over reciprocal space.[19] One must introduce an additional mechanism to account for this smearing out of the peaks. Adding positional disorder to the model by letting the phase shift vary over a range ϵ about the mean of 0.6 as shown in Fig. 8 will produce a Q-dependent broadening.[19] The dotted lines in the reciprocal space diagram indicate schematically how this broadening develops. The included angle between these dotted lines is proportional to ϵ and the length of the intersection with successive sheets gives the width of the short-range-order peaks. Hence, by adjusting ϵ one can wash out any structure in the second sheet while retaining the observed modulation of the first one. There are additional consequences[20] of this positional disorder which we were unaware of during the course of these experiments and these will be investigated in the future.

B. Long-range order

1. One set of mercury chains

Below 120 K two strong Bragg reflections at $(3 - \delta, 1 \pm \delta, 0)$ appear in the scan presented in Fig. 5, signaling the onset of long-range order in the chains parallel to the [100] direction. A general survey of that part of reciprocal space

associated with these mercury chains indicates that the Bragg peaks arising from the ordering can be indexed as $[h(3-\delta), k, l]$, $h+k+l=2n$, based on the host lattice unit cell. Figure 9 illustrates the nature of this long-range ordering. If one puts the mercury atoms belonging to the $z=0$ chains exactly in phase and shifts those at $z=\frac{1}{2}$ by $\frac{1}{2}a_{Hg}$ as shown in the basal projection of the mercury chains parallel to the [100] direction in the upper half of Fig. 9(a), then one expects peaks at $(h(3-\delta),\ k,\ l)$, $h+k+l=2n$ as indicated in the reciprocal-space diagram in the lower half of Fig. 9(a). Adding a phase shift of $\pm\delta a_{Hg}$ for neighboring chains at the $z=0$ level and maintaining the body-centering condition for the $z=\frac{1}{2}$ mercury chains leads to two monoclinic unit cells whose basal plane projections are shown in the upper half of Figs. 9(b) and 9(c). The lower half of the figures gives the reciprocal space diagram associated with the two unit cells and indicates the origin of the $\pm\delta$ displacements of the Bragg peaks relative to those shown in Fig. 9(a). Hence, assuming the presence of two kinds of domains with phase shifts of $+\delta$ and $-\delta$, respectively, one can

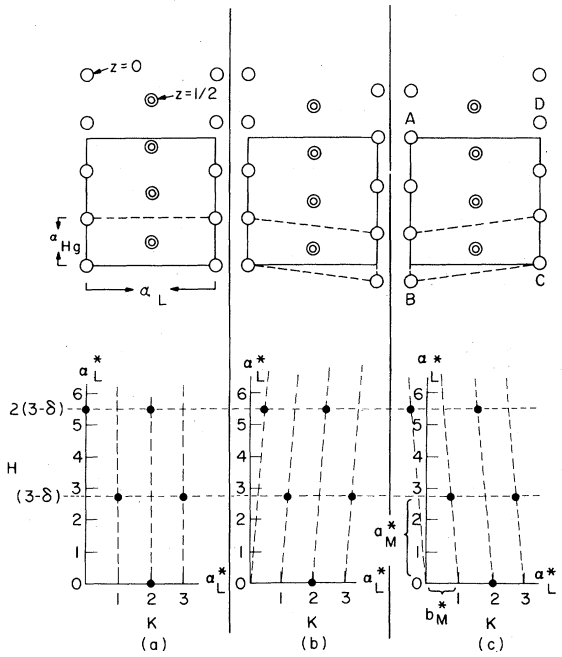

FIG. 9. (a) Upper half shows a basal plane projection of the Hg atoms in a set of parallel chains with zero phase shift between chains at $Z=0, \frac{1}{2}$, respectively. The resulting body-centered orthogonal unit cell is shown by the dashed line. The lower half of the figure shows the reciprocal lattice for this unit cell and the expected Bragg peaks (dote) for this type of ordering. (b) and (c) indicate the modification of both the direct and reciprocal spaces when the phase shift between chains is $+\delta_{Hg}$ and $-\delta a_{Hg}$, respectively.

account for the observed Bragg reflections associated with the mercury chains parallel to the [100] direction.

The fact that δ (in the host lattice units) describes *both* the position of the sheets δ_0 and the position of the Bragg reflections δ_1 along the sheets was determined by an accurate measurement of the position of the $(6-2\delta_0,\ 2\delta_1,\ 0)$ reflection. At 80 K, we found $\delta_0=0.209\pm0.004$ and $\delta_1=0.210\pm0.004$, so that within experimental error $\delta_0=\delta_1=\delta$. We have also checked that there are peaks for $l\neq0$ by observing the $(3-\delta,\ \pm\delta,\ 1)$ reflections.

In the disordered state at room temperature, the average structure of the mercury sublattice is tetragonal as is the host lattice. In the ordered state the mercury sublattice becomes monoclinic with a_M^* and b_M^* indicated in Fig. 9(c), with the unique monoclinic axis $c_M^*=c_L^*$. One would expect that this distortion of the mercury sublattice would induce a corresponding distortion of the host lattice. If one examines the relation between the mercury and host lattices one finds, as can be seen in the direct space diagram of Fig. 9(c), that the separation between mercury ions labeled A and C is $\sqrt{2}\ a_L$, but is greater than $\sqrt{2}\ a_L$ for ions B and D. A monoclinic distortion of the host lattice would lower the overall energy of the total system. The resulting deformation of the host lattice would be expected to reduce the tetragonal angle in the case of Fig. 9(c) and increase it for the domain represented by Fig. 9(b). Such a monoclinic distortion of the host lattice was indeed observed below 120 K. The host lattice formed two domains with $\beta^*=89.9°$ for the domain represented in Fig. 9(c) and $\beta^*=90.1°$ for the other domain. The indexing of the positions of the long-range-order Bragg peaks should properly be done using the monoclinic coordinate system of the corresponding host lattice, but this correction is very small and has been neglected.

Since the body-centered monoclinic unit cell we have used to describe the ordering of the mercury chains does not form a Bravais lattice,[21] it is necessary to transform the unit cell to a triclinic one containing one Hg atom per unit cell in order to calculate the structure factor of the long-range-order peaks properly. The assumption that only the Hg atoms contribute can then be checked with the observed intensities shown in Fig. 10 for one domain at 80 K. These intensities have been put on an absolute scale by measuring several Bragg reflections involving the host lattice only and obtaining a scale factor. Previously determined[3,12] positional parameters were used for this purpose. The intensities shown in Fig. 10 were also corrected for the Lorentz factor and absorption.[22]

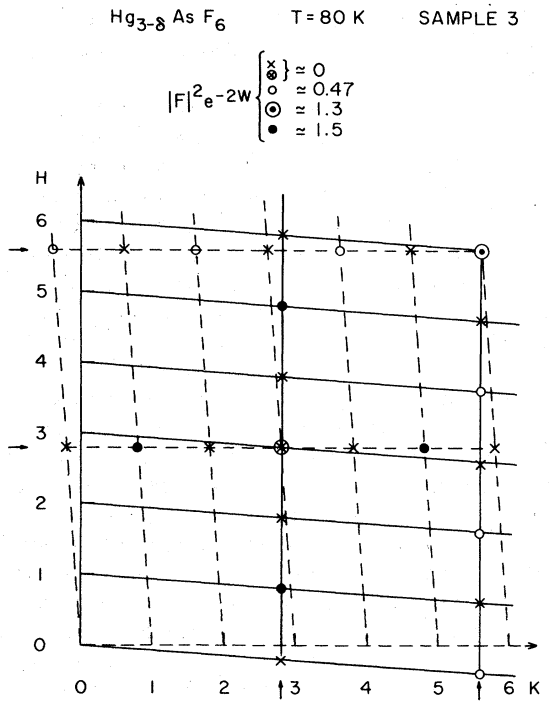

FIG. 10. Reciprocal-space diagram of $\{00l\}$ zone at 80 °K showing δ peaks for the two sets of orthogonal chains of one domain. The intensities $|F|^2e^{-2W}$ have been put on an absolute scale.

The measured intensities within a given sheet are constant within the 25% experimental accuracy resulting from uncertainties in the absorption correction and extinction. However, there is a large decrease in intensity from the first to the second sheet, indicating a large anisotropic Debye-Waller factor resulting from fluctuations along the chain direction. After correcting for the Debye-Waller factor, one obtains a constant structure factor $|F| \simeq 1.5$ in reasonable agreement with the tabulated[23] coherent scattering length of mercury, namely, 1.27×10^{-12} cm.

The experimental results yield an anisotropic Debye-Waller factor $W=B(\sin\theta/\lambda)^2$ with θ the scattering angle and λ the wavelength; W is small and undetectable perpendicular to the chain, but large along the chain. At 80 K, $B \simeq 5.5$ Å^2, a value similar to that found in rare-gas compounds. There are several possible explanations for this unusually large thermal factor. A study at much lower temperatures could distinguish among them and this will be done in later experiments.

2. *Two sets of mercury chains*

We have so far discussed one set of chains parallel to the [100] direction and the superlattice formed from these chains. A similar superlattice (once again neglecting the slight monoclinic distortion of the host lattice) is formed from the orthogonal set of chains parallel to the [010] direction. The remaining structural feature is the determination of the phase relationship between the two sets of perpendicular chains. An understanding of the coupling between these orthogonal sets of chains yields, as we shall see below, a simple picture of the chain-chain interaction in $Hg_{3-\delta}AsF_6$.

Let us begin by asking the question why the particular value of phase shift δa_{Hg} is adopted by the chains. At first, we thought this was somehow connected with the interaction between the host lattice and the parallel chains of mercury ions. It was pointed out to us by Axe[20] that this could not be so. It can be shown in general that two interpenetrating lattices can interact only if they share common reciprocal lattice points. Since the mercury lattice is incommensurate with respect to the host lattice, the chains cannot interact with the host no matter what the choice of phase shift. Therefore the selection of δa_{Hg} as the phase shift must be the result of the interaction between the perpendicular sets of chains.

As a particular example, let us consider the domain illustrated in Fig. 10. The indexing of the superlattice peaks (based on the host lattice unit cell) is given by $(h(3-\delta),\ k-h\delta,\ l)$ for the substructure generated by the mercury chains parallel to the [100] direction and by $(h-k\delta,\ k(3-\delta),\ l)$ for the substructure made up of the orthogonal set of chains. As can be seen from this figure there are Bragg peaks which are common to both structures, namely, those with indices $(m(3-\delta),\ m(3-\delta),\ 0)$. This sharing of reciprocal lattice points is possible only because the phase shift between neighboring parallel chains is δa_{Hg}, since the *position* of the sheets also depends on δ. We are thus led to conclude that the choice of phase shift for the ordering is brought about by the perpendicular chain-chain interaction. In fact, the phase shift of δa_{Hg} yields the maximum number of overlapping peaks.

We now turn to the question of the relative phasing of the two substructures of Fig. 10. Examination of the observed intensities shows that the $(3-\delta,\ 3-\delta,\ 0)$ peak is absent while the $(6-2\delta,\ 6-2\delta,\ 0)$ peak is approximately three times as intense as the other Bragg peaks in the same sheet. This indicates that the planes of both substructures which are perpendicular to the [110] direction of the host lattice are arranged so that there is destructive interference for the $(3-\delta,\ 3-\delta,\ 0)$ peak and thus constructive interference for the $(6-2\delta,\ 6-2\delta, 0)$ peak. This leads to the relative phasing of the two substructures indicated in Fig. 11. The

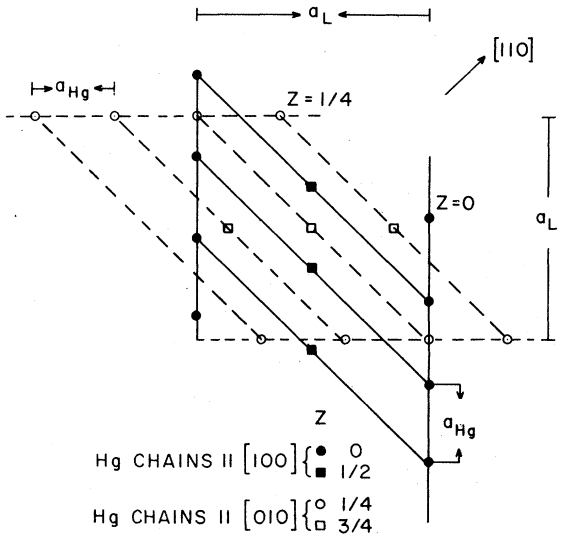

FIG. 11. Basal plane projection of the Hg atoms for the two sets of orthogonal chains showing the relative phasing required to explain the observed intensities of those peaks common to one domain.

planes of such substructure which contribute to the $(3-\delta, 3-\delta, 0)$ reflection are shown and these are displaced relative to each other so that there is destructive interference. This of course puts them in phase for the second reflection which should be four times as intense as the other Bragg reflections on the same sheet because two substructures contribute to the structure factor. This is in fair agreement with the observed increase of three.

There is another aspect of the existence of common reciprocal lattice points for the two mercury substructures which we will now consider. In the discussion of the structure of the ordered phase for one set of parallel mercury chains, ie., one substructure, we noted that the phase shift δa_{Hg} could be either positive or negative and that this led to the formation of two domains. The same choice of sign exists for the other mercury substructure, the parallel mercury chains orthogonal to the first set, so that there are in principle, four possible domains for the complete system. However, unless the phase shifts are properly coupled in the two substructures, there will be no reciprocal lattice points in common and hence no interaction between the substructures. This coupling of the sign of the phase shift would restrict the number of domains to two. The monoclinic distortion of the host lattice accompanying the onset of long-range order can be used to show that there are indeed only two domains. As previously mentioned this distortion also leads to two domains for the host lattice with a monoclinic angle of 89.9° and 90.1°, respectively. This distortion is sufficiently large so that one can identify the superlattice peaks with a particular host domain. This identification enables one to establish that there is a unique sign for the phase shift of the two mercury substructures in a given host domain and thus there are only two domains which are the ones with reciprocal lattice points in common.

C. 2δ satelites

The previous discussion has described the disordered and ordered structures of the mercury sublattice and noted a slight monoclinic distortion of the host lattice. The occurrence of these two separate incommensurate sublattices should lead to a modulation of both sublattices as a result of their mutual interaction. Indeed, this type of modulation has been observed recently for systems with interpenetrating sublattices.[15,16] We have looked for and found additional satellite peaks which indicate a modulation of the mercury sublattice, but have found no evidence for any modulation of the host sublattice.

Figure 12 shows the distribution of some of these satellites in the $\{0k0\}$ zone. They can all be indexed as $(h \pm 2\delta_2, 0, l)$ reflections and appear about all the allowed $(h0l)$ Bragg peaks. Accurate measurements of the positions of these satellites indicate that $\delta_2 = \delta$. Estimates of the integrated intensities, corrected for the Lorentz factor and absorption, indicate clearly that these intensities I

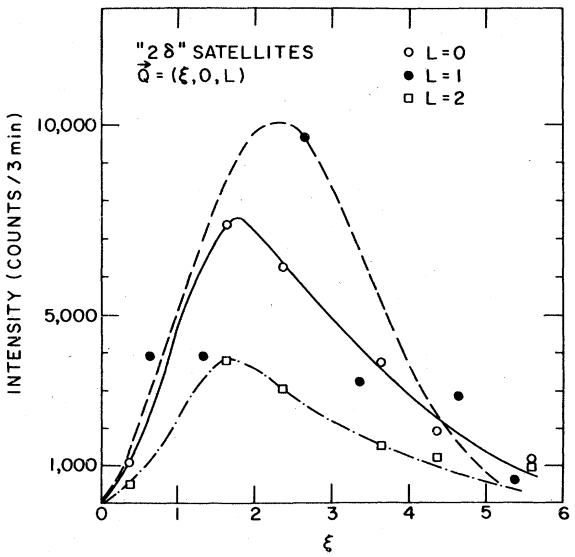

Fig. 12. Observed integrated intensities for a set of 2δ satellites. The lines are merely intended as a guide to the eye.

do not follow the structure factor of the associated Bragg peak. Instead, they follow a simple rule, $I \propto (\vec{Q}\cdot\vec{u})^2 e^{-\beta Q^2}$, the product of a displacive term with a polarization $\vec{u}$ in the (010) plane and a Debye-Waller term, $e^{-\beta Q^2}$. The rapid fall-off of intensity at large Q seen in Fig. 12 is the result of a large value for β which, from observations of the temperature dependence of one of these satellites, must be attributed mainly to static disorder. Similar results are found in the $\{h00\}$ zone. In the $\{00l\}$ zone, however, the 2δ satellites appear only along the [100] and [010] directions, i.e., only about those Bragg reflections whose structure factor contains a contribution from the mercury chains. There are no detectable satellites associated with the δ_1 peaks. The fact that the 2δ satellites are associated only with those Bragg peaks with a mercury contribution to the structure factor together with the observation that the 2δ displacement is perpendicular to the particular set of mercury chains involved in the Bragg peak enables one to conclude unambiguously that these satellites arise from a lateral modulation of the position of the parallel chains relative to each other. We have no satisfactory model of an interaction which would lead to this type of modulation and to the choice of $2\delta a_L^*$ as the propagation vector.

We have also measured the temperature dependence of the intensity of the $(2+2\delta, 0, 0)$ satellite and this is shown in Fig. 13. Its first appearance coincides with the ordering temperature of the mercury chains. Figure 13 also shows a comparison with the temperature dependence of the intensity of the $(3-\delta, 1-\delta, 0)$ peak which measures the degree of phase ordering of the chains.

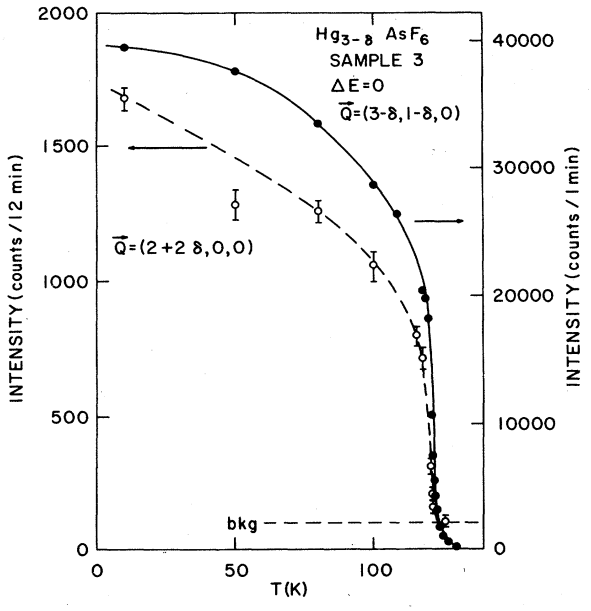

FIG. 13. Temperature dependence of the $(2=2\sigma, 0, 0)$ reflection (2σ satellite) compared with the $(3-\delta, 1-\delta, 0)$ reflection (σ satellite). The lines are to guide the eye.

V. SUMMARY

In this article, we have reported a detailed study of the polymercury cation compound $Hg_{3-\delta}AsF_6$ using elastic neutron scattering. This study and related earlier work have revealed several new aspects in the temperature dependence of the structure of this unusual incommensurate chain compound.

(a) The intrachain Hg-Hg distance is incommensurate with that of the host lattice.

(b) At room temperature the mercury chains are randomly phased forming a set of independent 1D lattices (with 1D phonon excitations) arranged within the host lattice.

(c) On cooling, phase order develops between the Hg chains. First, short-range order begins to grow because of the interaction between parallel chains. Then, at about 120 K, a different long-range order is established which arises from the interaction between the two orthogonal sets of chains.

(d) Finally, in the ordered state an additional incommensurate modulation of the lateral position of the chains develops.

The $Hg_{3-\delta}AsF_6$ compound opens a new class of exotic materials with unusual structural and electronic properties. Similar phenomena can be expected in other systems with quasi-one-dimensional elastic properties.

ACKNOWLEDGMENTS

We are especially grateful to Graheme Williams for his collaboration in the crystallographic computer calculations. Many helpful discussions with S. Aubry, R. Comes, V. J. Emery, R. Spal, C. K. Chiang, S. J. LaPlaca, J. M. Williams, and A. J. Schultz are also acknowledged. We are especially indebted to John Axe for many informative discussions of the theoretical model he and V. J. Emery have developed for this system.[24] Most of this paper was completed before the theoretical study was finished. Further experiments are planned to check the predictions of this new theory. Work at Brookhaven National Laboratory performed under the auspices of the U. S. Department of Energy. Work at the University of Pennsylvania supported by the NSF-MRL Program (DMR 76-00678) and by the NSF (MPS 73-04771-A1).

*Permanent address: Laboratoire de Physique des Solides, Associé au CNRS, Université Paris-Sud, 91405 Orsay, France.
†Department Physics, University of Pennsylvania.
‡Department of Chemistry, University of Pennsylvania.

[1] *Low Dimensional Cooperative Phenomena,* edited by H. J. Keller (Plenum, New York, 1975); Lecture Notes in Physics, Vol. 34; *One-Dimensional Conductors,* edited by H. J. Keller (Springer, New York, 1975); A. J. Berlinsky, Contemp. Phys. 17, 331 (1976); J. J. Andre, A. Bieber, and F. Gautier, Ann. Phys. 1, 145 (1976); *Chemistry and Physics of One-Dimensional Metals,* edited by H. J. Keller (Plenum, New York, 1977).
[2] B. D. Cutforth, W. R. Datars, R. J. Gillespie, and A. Van Schyndel, Adv. Chem. Ser. 150, 56 (1976).
[3] I. D. Brown, B. D. Cutforth, C. G. Davies, R. J. Gillespie, P. R. Ireland, and J. E. Vekris, Can. J. Chem. 52, 791 (1974).
[4] B. D. Cutforth, Ph.D. thesis (McMaster University, Hamilton, Ontario, 1975) (unpublished).
[5] B. D. Curforth, W. R. Datars, A. Van Schyndel, and R. J. Gillespie, Solid State Commun. 21, 377 (1976).
[6] C. K. Chiang, R. Spal, A. Denenstein, A. J. Heeger, N. D. Miro, and A. G. MacDiarmid, Solid State Commun. 22, 293 (1977).
[7] E. S. Koteles, W. R. Datars, B. D. Cutforth, and R. J. Gillespie, Solid State Commun. 20, 1129 (1976).
[8] D. L. Peebles, C. K. Chiang, M. J. Cohen, A. J. Heeger, N. D. Miro, and A. G. MacDiarmid Phys. Rev. B 15, 4607 (1977).
[9] E. Ehrenfreund, P. R. Newman, A. J. Heeger, N. D. Miro, and A. G. MacDiarmid, Phys. Rev. B 16, 1781 (1977).
[10] T. Wei, A. F. Garito, C. K. Chiang, and N. D. Miro, Phys. Rev. B 16, 3373 (1977).
[11] R. Spal, C. K. Chiang, A. Denenstein, A. J. Heeger, N. D. Miro, and A. G. MacDiarmid, Phys. Rev. Lett. 39, 650 (1977).
[12] A. J. Schultz, J. M. Williams, N. D. Miro, A. G. MacDiarmid, and A. J. Heeger, Inorg. Chem. 17, 646 (1978).
[13] Brookhaven National Laboratory Crystallographic Computing Library.
[14] J. P. Pouget, S. K. Khanna, and R. Comés (unpublished).
[15] S. J. LaPlaca, P. W. R. Corfield, R. Thomas, and B. A. Scott, Solid State Commun. 17, 635 (1975).
[16] C. K. Johnson and C. R. Watson, J. Chem. Phys. 64, 2271 (1976).
[17] J. M. Hastings, J. P. Pouget, G. Shirane, A. J. Heeger, N. D. Miro, and A. G. MacDiarmid, Phys. Rev. Lett. 39, 1484 (1977).
[18] N. D. Miro, A. G. MacDiarmid, A. J. Heeger, A. F. Garito, C. K. Chiang (unpublished).
[19] See e.g., A. Guinier, *X-Ray Diffraction* (Freeman, San Francisco, 1963).
[20] J. Axe (private communication).
[21] *Internationsl Tables for X-Ray Crystallography,* (Kynoch, England, 1969), Vol. I, p. 246.
[22] Computer programs obtained from Brookhaven National Laboratory Crystallographic Computing Library.
[23] G. E. Bacon, Acta Crystallogr. A28, 357 (1972).
[24] V. J. Emery and J. Axe (unpublished).

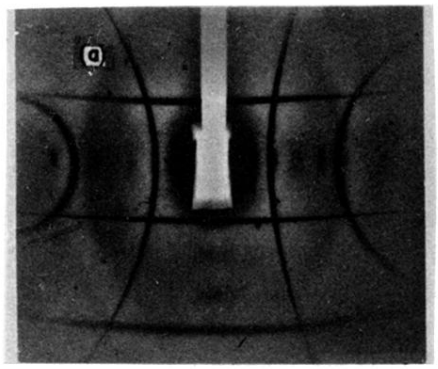

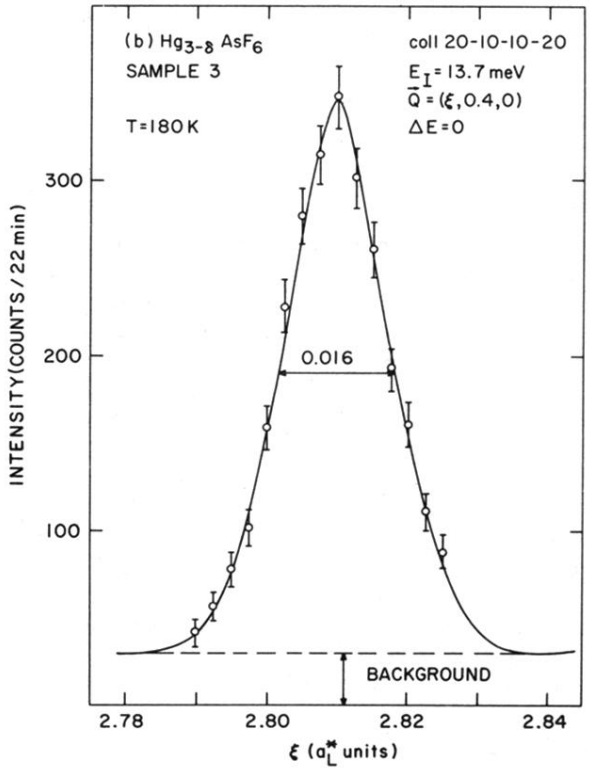

FIG. 3. (a) Diffuse x-ray pattern of $Hg_{3-\delta}AsF_6$ at room temperature. The incident beam is along the c_L^* direction (the subscript L refers to the host lattice). The curvature of the lines is the result of the flat plate geometry of the film (from Ref. 14). (b) (ξ, 0.4, 0) elastic neutron scan through the first diffuse sheet at 180 K. The width is resolution limited indicating an intrachain coherence length greater than 400 Å.